IEEE Access
Multidisciplinary | Rapid Review | Open Access Journal

Received September 29, 2020, accepted October 14, 2020, date of publication October 26, 2020, date of current version November 6, 2020.

Digital Object Identifier 10.1109/ACCESS.2020.3033717

Embeddable Structure for Reducing Mutual Coupling in Massive MIMO Antennas

YUE QIN, RONGLIN LI, (Senior Member, IEEE), AND YUEHUI CUI, (Member, IEEE)
School of Electronic and Information Engineering, South China University of Technology, Guangzhou 510641, China

Corresponding author: Yuehui Cui (eeyhcui@scut.edu.cn)

This work was supported in part by the National Natural Science Foundation of China under Grant 62071185 and Grant 61871194, and in part by the Department of Science and Technology of Guangdong Province under Grant 2019A1515011410.

ABSTRACT An embeddable decoupling structure is proposed for massive multiple-input-multiple-output (M-MIMO) antennas in this paper. The embeddable decoupling structure is made up of an end-folded metal strip and a pair of C-shaped metal strips. By introducing the embeddable decoupling structure near two closely spaced dipole antennas, additional coupling can be generated to counterbalance the original mutual coupling between the dipole antennas. The decoupling structure is firstly designed for a 1×2 MIMO antenna, which can provide a reduction of about 5 dB for the mutual coupling. Then, an evolutional decoupling structure is designed, which is composed of a pair of inverted U-shaped metal strips and two parallel reversed C-shaped metal strips. The evolutional decoupling structure is employed in a 3×3 MIMO antenna operating in 5G bands to demonstrate its capability of decoupling. An average reduction of about 10 dB on mutual coupling is obtained over 3.3-4.5 GHz (30.8%). Moreover, it is found that the deteriorated radiation patterns due to the mutual coupling are improved. The decoupling structure can be totally embedded in a M-MIMO antenna, which has no increase in the antenna volume. The proposed decoupling structure exhibits advantages of radiation pattern distortion alleviation, wideband, embeddable, and dual-polarized capabilities for M-MIMO applications.

INDEX TERMS Decoupling method, M-MIMO antenna, decoupling structure, dual-polarized antenna.

I. INTRODUCTION

Due to the advantages in high spectral efficiency and large system capacity, the massive multiple-input-multiple- output (M-MIMO) is a key technology for the fifth generation and beyond (5G & B5G) in mobile communications. M-MIMO antennas with the capability of beamforming play an important role for the realization of a data rate 20 times faster and a latency about 30 times lower than those of the 4G LTE cellular technology. As it is well known that the more antennas the transmitters/receivers are equipped with, the more signal channels can be provided, thus there would probably be tens to hundreds of antenna elements accommodated in a M-MIMO antenna. From the viewpoint of wide-angle beam scanning, system miniaturization and space saving, closely spaced antenna elements are placed in a constrained space. Strong mutual coupling would occur among the antenna elements, which may cause severe harms to the wireless communication systems. It has been demonstrated in several previous articles that a M-MIMO system can provide high spectral efficiency and large capacity only with low mutual coupling among antenna elements [1]–[3]. Therefore, reducing the mutual coupling has become a critical issue for M-MIMO antennas.

An investigation of the effect of mutual coupling on data throughput shows that a quasi-saturation point of mutual coupling between a pair of MIMO antenna is -20 dB [4]. It is demonstrated that the active voltage standing-wave ratio (VSWR) may be more than 2 at the mutual coupling level of -20 dB. An even less mutual coupling level is required for VSWR lower than 2. Therefore, the mutual coupling level for M-MIMO antennas should be no higher than -20 dB.

A lot of efforts have been devoted to reducing the mutual coupling in M-MIMO antennas. The previous decoupling structures can be roughly divided into four categories. The first is the metamaterial structures, such as inserting a metasurface shield [5], [6], a polarization rotator wall [7], a 3D meta-structure resonator [8] or a metasurface wall [9] between antenna elements. However, those metamaterial

The associate editor coordinating the review of this manuscript and approving it for publication was Lu Guo.

structures are made up of periodical metallic cells, leading to a large size, which may not be suitable for M-MIMO antennas. Metasurfaces for decoupling are usually applied above antenna elements [10]–[12]. The metasurfaces achieve suppressions of mutual coupling over a bandwidth less than 16%, which is not wide enough for 5G bands. The second category is employing decoupling networks [13]–[20] between the input ports of antenna elements. But those elaborately designed decoupling networks may be hard to be implemented on a large scale within a limited volume. The third category is introducing resonating metal decoupling structures between antenna elements, such as asymmetrical coplanar strip wall [21], H-shaped conducting wall [22], and near-field resonator [23]. However, those decoupling structures cannot be employed for dual-polarized antennas. Recently, a decoupling ground is proposed for reducing the coupling caused by coupling currents flowing on the shared ground [24], which can be regarded as the fourth category. The decoupling is achieved by adjusting the shape of the ground under each antenna element to make the mutual coupling from the free space and the ground out of phase. Still, it is not easy for the decoupling ground to achieve wideband operation. Besides, most of the decoupling structures fail to alleviate the deterioration in radiation patterns, which is even more challenging. Therefore, it is desirable to develop a decoupling structure for M-MIMO antenna for the purpose of reducing mutual couplings between antenna ports as well as radiation patterns improvement without increasing any extra antenna volume.

In this paper, a theoretical analysis on the decoupling for two side-by-side or end-to-end dipoles with a parallel parasitic dipole has been carried out. It is revealed that the mutual coupling between dipole antennas can be reduced by introducing a parasitic dipole in parallel with them. For dual-polarized dipole-type MIMO antennas, the parasitic decoupling dipoles for side-by-side dipoles and end-to-end dipoles are combined to form embeddable decoupling structures to reduce the mutual coupling. Theoretical analysis is shown in Section II. The embeddable decoupling structure is developed in Section III. An evolutional embeddable decoupling structure is designed and accommodated for a 3×3 MIMO antenna in Section IV. Experimental results about the 3 × 3 MIMO antenna are displayed in Section V. Finally, a conclusion is drawn out in Section VI.

II. OPERATION PRINCIPLE

A. DECOUPLING FOR TWO SIDE-BY-SIDE DIPOLES

Two side-by-side dipoles with a half-wave length (λ/2) and separated by a distance d, namely Dip 1 and Dip 2, can be considered as a two-port network. The arrangement is shown in Figure. 1. The voltage-current relations can be expressed as

$$\begin{bmatrix} V_1 \\ V_2 \end{bmatrix} = \begin{bmatrix} Z_{11} & Z_{12} \\ Z_{21} & Z_{22} \end{bmatrix} \begin{bmatrix} I_1 \\ I_2 \end{bmatrix} \tag{1}$$

where V_1, V_2, I_1, and I_2 denote the voltages and currents on Dip 1 and Dip 2, respectively.

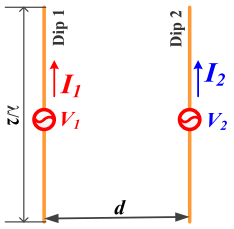

FIGURE 1. Two side-by-side coupled dipoles.

When the Dip 1 is driven with a voltage V_1 and the Dip 2 is short-circuited (i.e. $V_2 = 0$), the coupling current on Dip 2 is

$$I_{12} = I_2|_{V_2=0} = -\frac{Z_{21}}{Z_{22}} I_1. \tag{2}$$

Due to the reciprocity for antennas, the mutual impedance Z_{12} is equal to Z_{21}, which is given in [25] as

$$Z_{21} = j30 \int_0^L \left\{ \frac{\exp(-j\beta\sqrt{d^2+z^2})}{\sqrt{d^2+z^2}} \right\} \sin(\beta z) dz + j30 \int_0^L \left\{ \frac{\exp\left(-j\beta\sqrt{d^2+(L-z)^2}\right)}{\sqrt{d^2+(L-z)^2}} \right\} \sin(\beta z) dz \tag{3}$$

with $\beta = 2\pi/\lambda$. The input impedance of a λ/2 thin dipole is

$$Z_{22} = 73 + j42.5(\Omega). \tag{4}$$

Combining Equations (3) and (4) into Equation (2), the magnitude ratio and phase difference $\Delta\theta$ between I_1 and I_2 are obtained as

$$\left|\frac{I_{12}}{I_1}\right| = \left|-\frac{Z_{21}}{Z_{22}}\right| \tag{5a}$$

and

$$\Delta\theta = |\angle I_1 - \angle I_2| = |\angle - \frac{Z_{21}}{Z_{22}}|. \tag{5b}$$

From the above derivation, both the magnitude ratio and phase difference vary with the separation distance d. Figure 2 shows the phase difference $\Delta\theta$ varying with the distance d, which is obtained by calculation according to

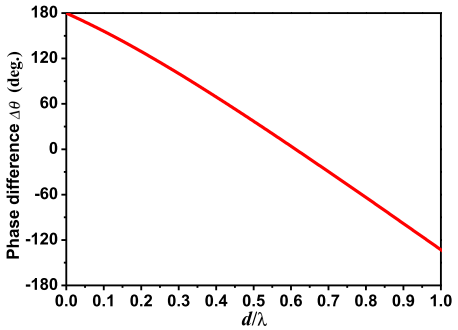

FIGURE 2. The phase difference of current I_1 and I_2.

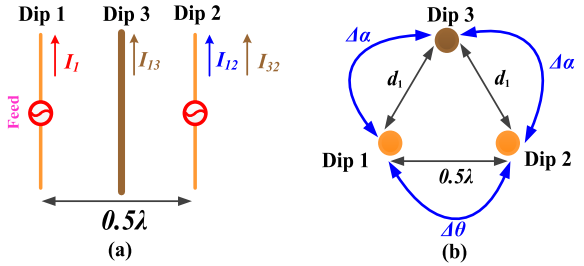

FIGURE 3. Two side-by-side coupled dipoles with the parasitic dipole.

the formulas (2)-(5) with the software *Matrix Laboratory (Matlab) v. 2016a.* (Figure 4, Figure 5, Figure 8 and Figure 9 are obtained in the same way.) Seen in Figure 2, the phase difference gradually decreases from about 180° to below 0° with the increase of the distance. The phase difference is 180° when the two dipoles are very close. This enables us to introduce a parasitic dipole at a different distance to counterbalance the original coupling effect.

The parasitic dipole Dip 3 is introduced in the middle of Dips 1 and 2 and moves along the perpendicular bisector. The distance between Dip 3 and Dip 1 or 2 is d_1. An additional coupling path from Dip 1 to Dip 2 is bridged by Dip 3. As shown in Figure 3(b), when the Dip 1 is driven, it causes direct coupling currents I_{12} and I_{13} on Dip 2 and Dip 3. The phase difference between I_1 and I_{12} is $\Delta\theta$ and that between I_1 and I_{13} is $\Delta\alpha$. Relayed by Dip 3, another coupling current I_{32} is also induced on Dip 2. Due to geometric symmetry, the phase difference between I_{13} and I_{32} is also $\Delta\alpha$. It is easy to extrapolate that the direct coupling on Dip 2 from Dip 1 can be cancelled out by the indirect coupling bridged by Dip 3 when I_{32} is out of phase with I_{12}. In other words, the parasitic dipole serves as a decoupling structure when

$$2\Delta\alpha - \Delta\theta = 180^\circ. \tag{6}$$

The phase differences can be optimized by changing the distance d_1. Figure 4 displays the phase difference $(2\Delta\alpha - \Delta\theta)$ varying with the distance d_1. The value of $(2\Delta\alpha - \Delta\theta)$ is found to be about 180° when d_1 is 0.27λ.

Due to the twice coupling, the indirect coupling path can be regarded as a cascade network, which is the two-port network of Dip 1 and 3 in cascade with the two-port network of Dip 3 and 2. Then, we have

$$I_{32} = -\frac{Z_{23}}{Z_{22}} \cdot I_{13} \tag{6a}$$

and

$$I_{13} = -\frac{Z_{31}}{Z_{33}} \cdot I_1. \tag{6b}$$

From the Equations (1) and (6), the magnitude ratio of I_{32} and I_{12} can be expressed as

$$\left|\frac{I_{32}}{I_{12}}\right| = \left|\frac{Z_{23}}{Z_{22}} \cdot \frac{Z_{31}}{Z_{33}} \cdot \frac{Z_{22}}{Z_{21}}\right|. \tag{7}$$

The Z_{ij} (i = 1, 2, 3 and j = 1, 2, 3) are the Z parameters of each two-port network. The magnitude ratio of I_{32} and I_{12}

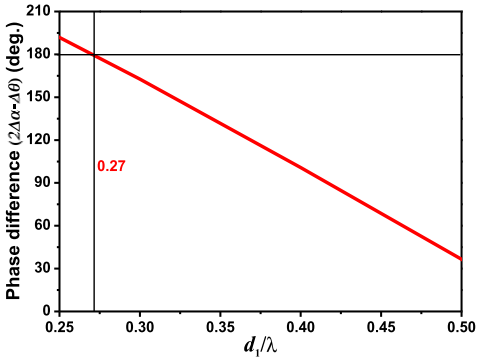

FIGURE 4. The variation of the value of $(2\Delta\alpha - \Delta\theta)$ with different d_1.

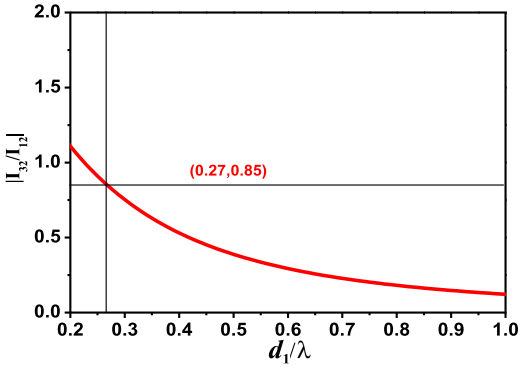

FIGURE 5. The ratio of the magnitude of I_{32} and I_{12} with the variation of d_1.

varying with distance d_1 is shown in Figure 5. It is 0.85 when d_1 is 0.27λ, which indicates that most of the direct mutual coupling between the two dipoles is cancelled by the indirect coupling from the parasitic dipole.

To verify the theoretical analysis, an investigation on the S parameters of the two half-wave dipoles with and without the parasitic dipole has been carried out. All the simulations were carried out with the software *Ansoft High Frequency Structure Simulator (HFSS) v. 15*. The S parameter |S21| is displayed in Figure 6. It is shown that there is a maximum improvement of more than 15 dB at the operation frequency when d_1 is 0.27λ. Note that when d_1 is greater than 0.43λ, the |S21| is almost the same with that without the parasitic dipole. This is because the value of $(2\Delta\alpha - \Delta\theta)$ is less than 90° where the current I_{12} and I_{32} tends to be in phase.

B. DECOUPLING FOR TWO END-TO-END DIPOLES

Rearrange the two half-wave dipoles to be end-to-end and separated by 0.6λ, which is shown in Figure 7. Similarly, a parasitic dipole is introduced along the perpendicular bisector between them at a distance d_2 to provide an additional coupling path for the purpose of decoupling. The three dipoles go through the same analysis process presented in Part A except that the mutual impedances between each pair of the dipoles are different with those for the dipoles in Figure 1. The mutual impedances between Dips 1&2, Dips 1&3 and Dips 2&3 are also given in [25] (See Appendix).

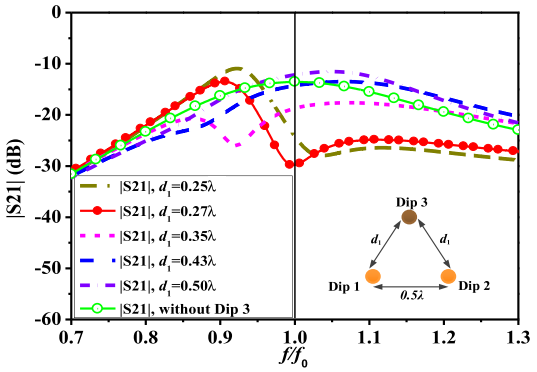

FIGURE 6. The S parameter |S21| of Dip 1 and Dip 2 with the variation of the distance d_1.

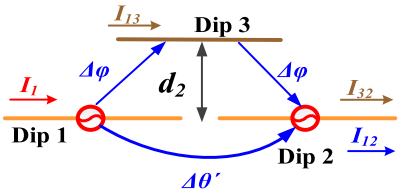

FIGURE 7. Two end-to-end coupled dipoles with the parasitic dipole.

When the Dip 1 is driven, it causes direct coupling currents I_{12} and I_{13} on Dip 2 and Dip 3, respectively. Relayed by Dip 3, there appears coupling current I_{32} on Dip 2. The phase difference between I_1 and I_{12} is $\Delta\theta'$. The phase difference between I_1 and I_{13} is $\Delta\varphi$, which is the same with the phase difference between I_{13} and I_{32}. The magnitude and the phase of the coupling currents are determined by the distance d_2. Therefore, by optimizing the distance d_2, the dipole Dip 3 can be placed in a proper position to function as a decoupling structure, where the induced coupling current I_{32} is out of phase with I_{12}. Figure 8 displays the phase difference varying with the distance d_2. The value of $(2\Delta\varphi - \Delta\theta')$ is found to be about 180° when d_2 is 0.17λ. The magnitude ratio of I_{32} and I_{12} varying with different distance d_1 is shown in Figure 9. When distance d_2 is 0.17λ, the magnitude ratio is about 1.35. Figure 10 displays the S parameter |S21| of Dip 1 and Dip 2 without and with Dip 3. The best isolation is found to be about 30 dB at the operation frequency, which is 13 dB better than that without the Dip 3.

Therefore, a qualitative knowledge about reducing mutual coupling between two closely spaced parallel dipoles by introducing a parasitic dipole in parallel with them in a proper distance can be established.

III. THE EMBEDDABLE DECOUPLING STRUCTURE

A two-element MIMO antenna is developed, which is made up of two dual-polarized bowtie dipole antennas. The bowtie dipole antenna is redesigned from the dual-polarized antenna presented in our previous publication [26]. The element space is 0.56λ_0, where λ_0 is the free space wavelength at 3.9 GHz. The MIMO antenna has a bandwidth of 3.3-4.5 GHz (30.8%) to cover the frequency bands of 3.3-3.6 GHz and 4.4-4.5 GHz for 5G applications in China and the 5G band of 3.6-4.2 GHz

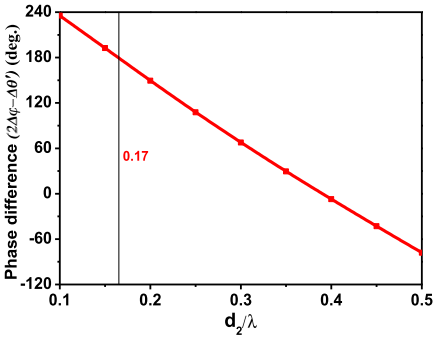

FIGURE 8. The variation of the value of $(2\Delta\varphi - \Delta\theta')$ with different d_2.

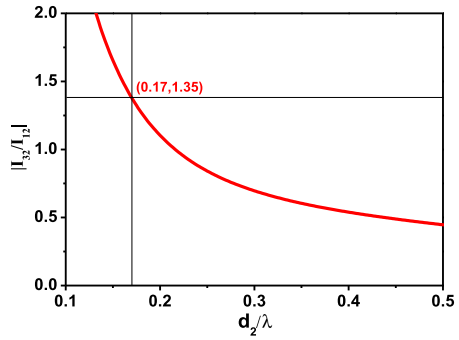

FIGURE 9. The ratio of the magnitude of I_{32} and I_{12} with the variation of d_2.

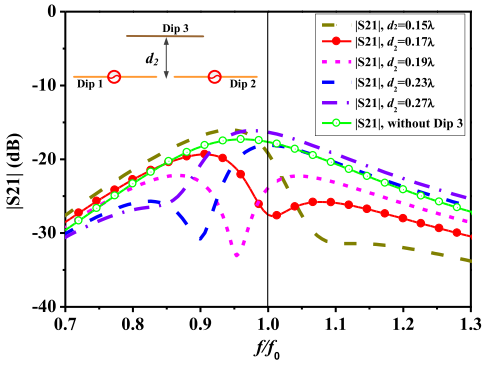

FIGURE 10. The effects of the distance d_2 on the S parameter |S21| of Dip 1 and Dip 2.

in Japan. The decoupling structure is illustrated in Figure 11. An end-folded metal strip is inserted between the dual-polarized bowtie dipole antennas as a transformation of the parasitic dipole introduced around two side-by-side dipoles. Two C-shaped strips is used to replace the parasitic dipole for the end-to-end dipoles. Both the bowtie dipole antennas and the strips are printed on a Rogers 4350B substrate with relative permittivity of 3.45 and a thickness of 0.508 mm. The end-folded and the C-shaped metal strips own a total length of 50 mm and 48 mm, respectively, which are about 0.65λ_0. The end-folded metal strip is placed 0.09λ_0 beneath the array and about 0.29λ_0 away from each dipole antenna. The C-shaped metal strip is positioned 0.1λ_0 under the dipole antennas.

The decoupling effects of the proposed decoupling structure on the S parameters of the two-element MIMO antenna

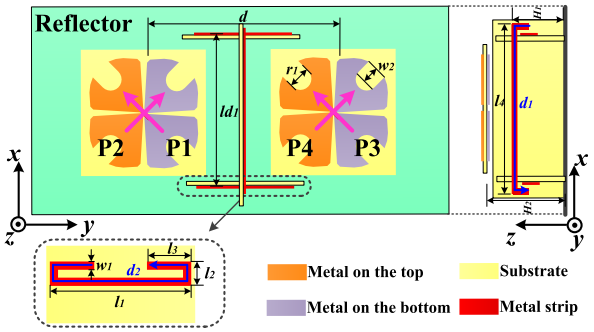

FIGURE 11. Geometry of the decoupling structure embedded within two dual-polarized bowtie dipole antennas. The optimized parameter values are as follows: $l_1 = 29$ mm, $l_2 = 5.5$ mm, $l_3 = 8$ mm, $l_4 = 42$mm, $ld_1 = 16$ mm, $H_1 = 16.5$ mm, $H_2 = 23$ mm, $w_1 = 2$ mm, $w_2 = 3.8$ mm, $r_1 = 3$ mm, and $d = 43.5$mm.

are displayed in Figure 12. As shown in Figure 12(a), with either end-folded strip or the two C-shaped strips, the mutual coupling can be reduced by about 3 dB for two parallel bowtie dipoles with the same polarization (co-pol. coupling). By introducing both the end-folded strip and two C-shaped strips, the mutual coupling is reduced by about 5 dB. In addition, the decoupling structure also contributes to the suppression of the mutual coupling between two orthogonal bowtie dipoles (x-pol. coupling). Seen in Figure 12(b), the x-pol. coupling is reduced by about 10 dB from about −15 dB to lower than −25 dB. Note that the proposed decoupling structure has slight influence on the return loss and isolation of each dual-polarized bowtie antenna. As shown in Figure 13, the 15-dB return losses (−|S11| or −|S22|) with or without the decoupling structure cover the same frequency band of 3.3-4.5 GHz; the isolation, i.e. −|S21| or −|S43|, are about 30 dB.

The current distributions on the two-element MIMO antenna with the end-folded metal strip or the C-shaped metal strip are exhibited in Figure 14. One of the bowtie dipoles is excited and the others are terminated with 50-Ω broadband loads. It is found that the currents on the end-folded metal strip and the C-shaped metal strip flow in the same way with the current on a dipole. The ends of the metal strips are folded for the purpose of miniaturization. At the folded ends, the currents are weak and flow in opposite directions.

The current distributions on the dual-polarized bowtie dipole antennas with the whole decoupling structure are plotted in Figure 15 in comparison with those without the decoupling structure. The coupling current on the unexcited dipoles is noticeably reduced due to the decoupling structure. It is verified that decoupling structure provides additional coupling path for counterbalancing the original mutual coupling between the two antennas.

IV. DUAL-POLARIZED MIMO ANTENNA WITH THE EMBEDDABLE DECOUPLING STRUCTURES

In a M-MIMO antenna, there are dozens of antenna elements. Each of the antenna elements at the corner only has two neighboring antenna elements. Each of the antenna elements

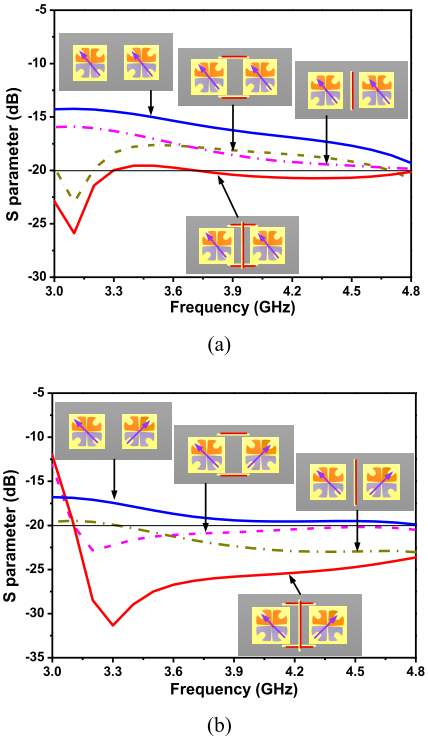

FIGURE 12. The effects of the end-folded metal strip, the C-shaped strips, and the proposed decoupling structure on the (a) co-pol. coupling and (b) x-pol. coupling.

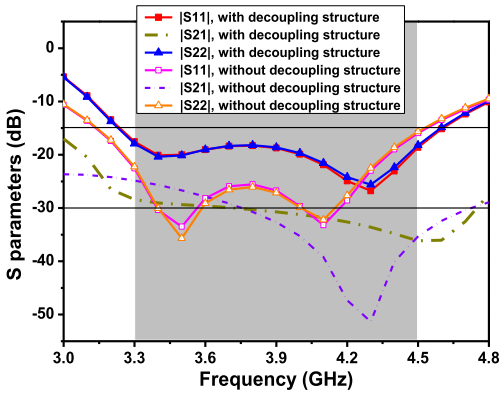

FIGURE 13. Simulated S parameters of the each dual-polarized bowtie dipole antenna with and without the decoupling structure.

on the edge has up to five neighboring antenna elements. Except the antenna elements at the corner or on the edges, each antenna element in a M-MIMO antenna is surrounded by eight other antenna elements and receives the strongest mutual coupling. The mutual coupling problem of the center antenna element of a 3×3 MIMO array is a typical mutual coupling issue in a M-MIMO antenna. In order to conduct an estimation on the effects of the decoupling structures, the decoupling structure is embedded in a nine-element MIMO antenna. As illustrated in Figure 16, nine wideband dual-polarized bowtie dipole antennas are arranged in a 3×3 MIMO array with an element spacing of $0.56\lambda_0$. The original decoupling structure presented in Section III is applied in the MIMO antenna at first. For every two adjacent antenna ele-

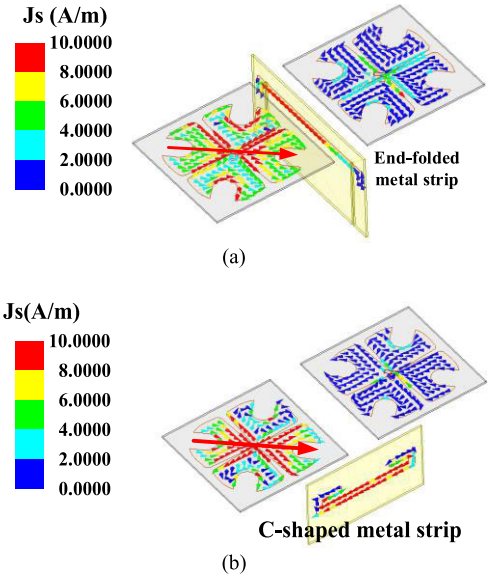

FIGURE 14. The current distributions on the two-element MIMO antenna and decoupling structures at 3.3 GHz: (a) with the end-folded metal strip and (b) with the C-shaped metal strip.

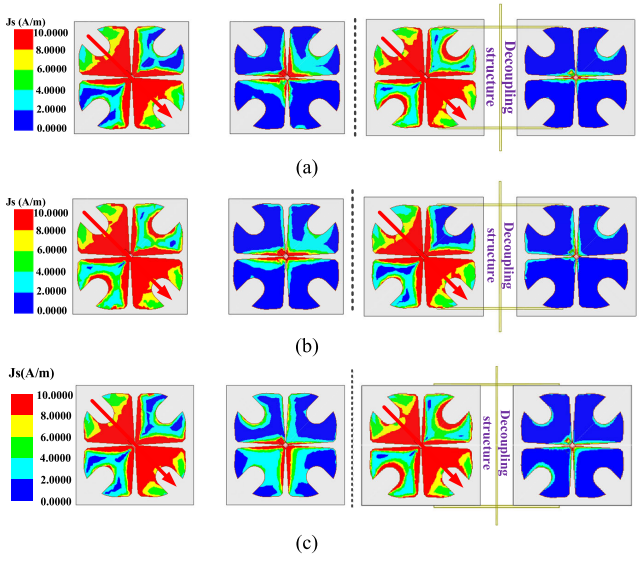

FIGURE 15. The current distributions on the two-element MIMO antenna and decoupling structures at: (a) 3.3 GHz, (b) 3.9GHz, and (c) 4.5GHz.

ments, there are C-shaped strips at each side. Between every two antenna elements, there is an end-folded metal strip. However, the original decoupling structure does not achieve a good performance as in a two-element MIMO antenna. It is understandable that the mutual coupling is more complex and severe in the nine-element MIMO antenna than that in the two-element MIMO antenna. An evolutional decoupling structure is then proposed for better suppression of mutual couplings both on S parameters and radiation patterns.

The evolutional decoupling structure is also shown in Figure 16. Between every two adjacent antenna elements, another metal strip is added beside the original end-folded metal strip, so that a much stronger additional coupling can

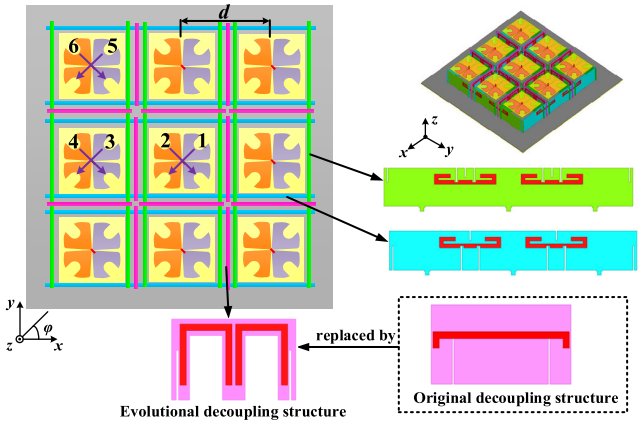

FIGURE 16. The configuration of the nine-element MIMO antenna with the original decoupling structures or the evolutional decoupling structures.

be provided to better counterbalance the mutual coupling between antenna elements. Each metal strip is folded to have a U shape, so that the evolutional decoupling structure can be easily embedded in the MIMO antenna.

The simulated results for the S parameters of the nine-element MIMO antenna without the decoupling structure, with the original decoupling structure or with the evolutional decoupling structure are presented in Figure 17. Due to symmetric geometry, there is no need to present all the S parameters for every antenna element in the M-MIMO antenna. The S parameters for the center element, one corner element and one element on the edge are plotted. The S parameters and radiation patterns of the center element are of important values for reference.

The co-pol. mutual coupling between the center element and its adjacent element, i.e. |S13| and |S24|, are plotted in Figure 17 (a). The co-pol. mutual coupling is up to −13 dB at about 3.9 GHz without the decoupling structures. After the original decoupling structure is introduced, the co-pol. mutual couplings at the frequency band of 3.3-4.0 GHz are still higher than −20 dB. The evolutional decoupling structure brings out a suppression of mutual coupling of 5 to 20 dB over the frequency band of 3.3-4.5 GHz. The x-pol. mutual coupling between the center element and its adjacent element, i.e. |S14| or |S23|, are plotted in Figure 17(b). A decrease of up to 10 dB for the x-pol. mutual coupling appears around 3.3 GHz, which is attributed to the evolutional decoupling structure. Seen in Figure 16 (c) & (d), the dual-polarized bowtie antenna has a bandwidth over 3.3-4.5 GHz for |S11| or |S22| <-15 dB. The original decoupling structure has little help on impedance matching. After the evolutional decoupling structure is employed, the impedance bandwidth maintains covering 3.3-4.5 GHz. The isolation, i.e., −|S21|, is better than 30 dB with and without the decoupling structures.

The evolutional decoupling structure also exhibits attractive features in alleviating the distortion in radiation patterns. The simulated radiation patterns and antenna gains with and without the evolutional decoupling structure are

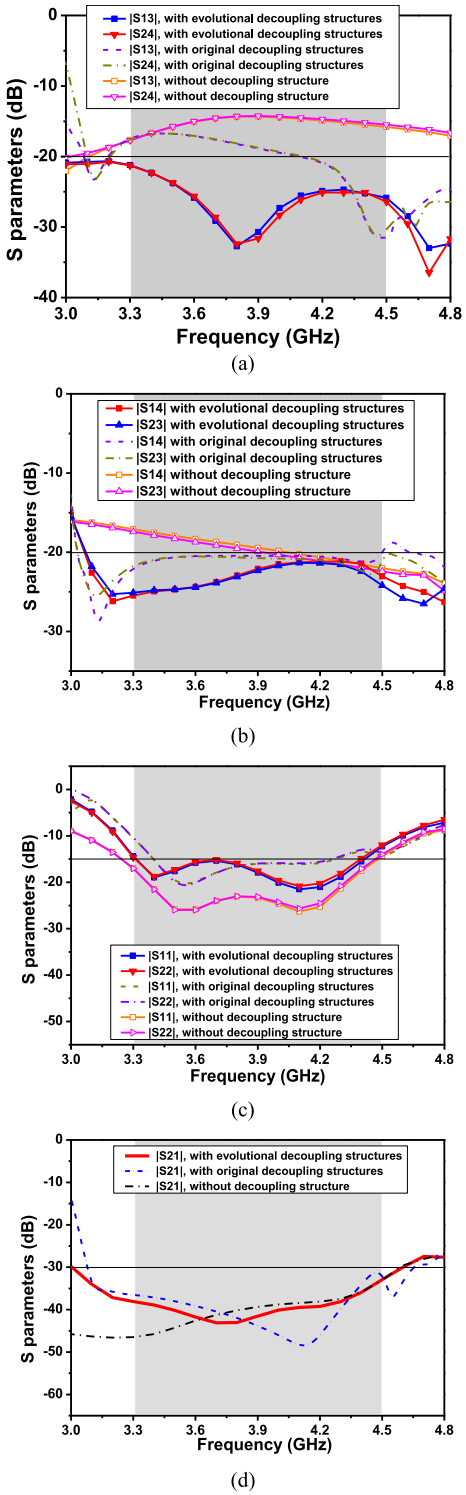

FIGURE 17. Simulated S parameters of the nine-element MIMO antenna without the decoupling structure, with the original decoupling structures or with the evolutional decoupling structures: (a) |S13| and |S24|, (b) |S14| and |S23|, (c) |S11| and |S22| for the center element, and (d) |S21| for the center element.

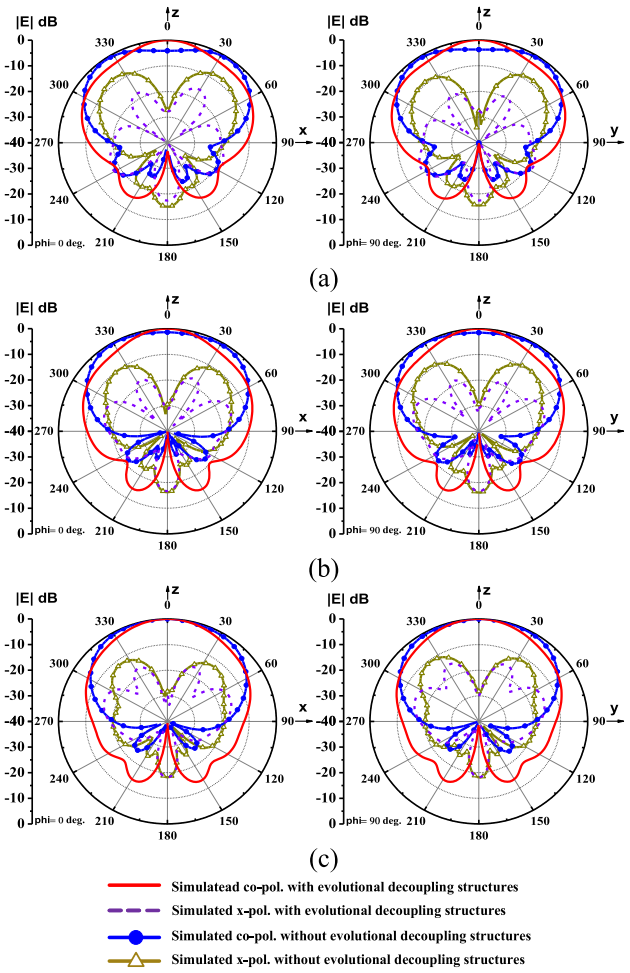

FIGURE 18. Simulated radiation patterns of the center antenna element with or without the evolutional decoupling structures at: (a) 3.3GHz, (b) 3.6 GHz, and (c) 3.9 GHz.

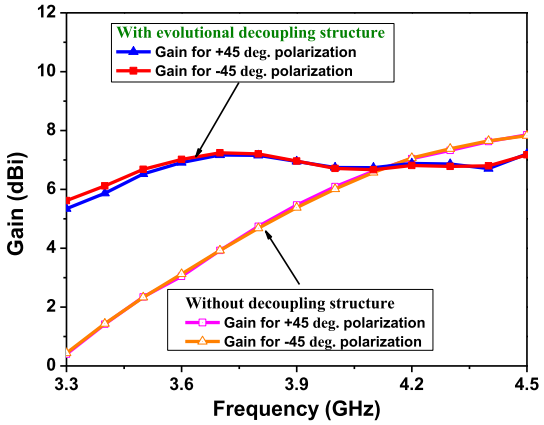

FIGURE 19. Simulated gain of the center antenna in the MIMO antenna.

shown in Figure 18 and Figure 19, respectively. Note that the radiation patterns for the center antenna element in −45° polarization are the same with those for +45° polarization because of symmetric geometry. Only the radiation patterns for the +45° polarization of the center antenna element are provided. Without the evolutional decoupling structure, there is an obvious dent in the main beam of the radiation patterns, see in Figure 18 (a) and (b). The dent in the main beam also leads to low antenna gain over the lower half of the operation band. With the evolutional decoupling structures,

the distortion of the radiation pattern is restored; the radiation patterns become symmetric and stable; and the antenna gain has risen to around 7 dBi. It is also found that the cross-polarization is improved to be around −15 dB by a maximum enhancement of 10 dB. The front-to-back (F/B) ratios with and without the evolutional decoupling structure are almost the same. It is well demonstrated that the evolutional decoupling structure can effectively reduce the mutual coupling for dual-polarized dipole-type M-MIMO antennas.

V. MEASUREMENT OF THE MIMO ANTENNA WITH THE DECOUPLING STRUCTURES

The nine-element MIMO antenna with the evolutional decoupling structures has been fabricated and measured. The prototype of the MIMO antenna is shown in Figure 20. The measurement for S parameters has been carried out using *Keysight PNA-L network analyzer N5230A*. The radiation patterns and antenna gains are measured with a *SG-64 SATIMO system*. The measured S parameters for the center element are shown in Figure 21 in comparison with the simulated results. Agreements are observed between the simulated and measured results. As shown in Figure 21(a), the impedance bandwidth for |S11| or |S22| < -15 dB covers the frequency band 3.3-4.5 GHz. The isolation, i.e., $-|S21|$, is shown in Figure 21(b), which is higher than 30 dB. As plotted in Figure 21(c)-(d), the co-pol. mutual coupling, i.e., |S13| or |S15|, is lower than −20 dB; the x-pol. mutual coupling, i.e., |S14|, is lower than −25 dB, the mutual coupling between two collinear dipoles, i.e., |S26|, remain lower than −20 dB. The measured radiation patterns for the center element are shown in Figure 22, which are in good agreement with the simulation. Stable unidirectional radiation patterns are achieved. It is shown in Figure 23 that the measured antenna gain is about 6.5 dBi for both ±45° polarizations. There is about a discrepancy about 0.3 dB between the measured and simulated results. This is due to the coaxial lines and the SMA connectors which have not been taken into consideration during the simulation. Figure 24 shows the measured efficiency of the center antenna element with the evolutional decoupling structure, which is about 80%. It is demonstrated that the evolutional decoupling structure can effectively reduce the mutual coupling for dual-polarized dipole-type M-MIMO antennas. The decoupling structure

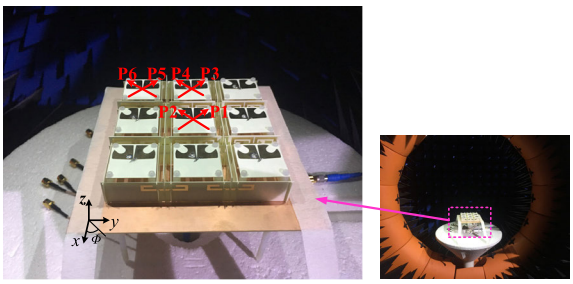

FIGURE 20. The fabricated 3 × 3 MIMO antenna.

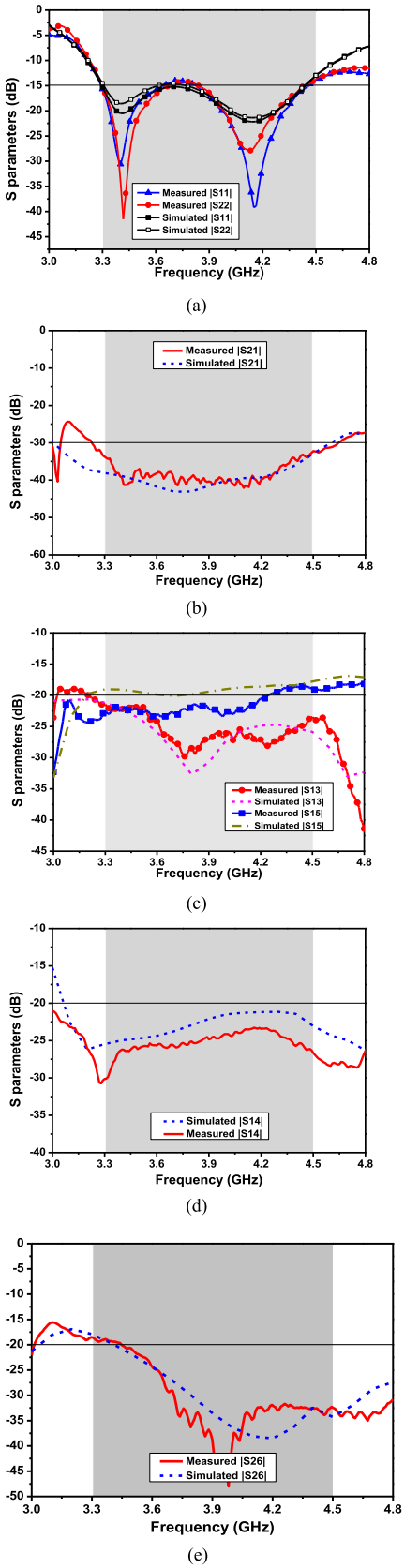

FIGURE 21. The measured S-parameters of the fabricated 3 × 3 MIMO antenna: (a) |S11|&|S22|, (b) |S21|, (c) |S13|&|S15|, (d) |S14|, and (e) |S26|.

TABLE 1. The comparison of the proposed decupling structure with other art-of-the-state decoupling structure.

Ref.	Type	Array Config.	Pol.	BW (GHz)	Co-pol. (dB)	X-pol. (dB)	Element Space (λ_c)	RPDA	Embeddable
[5]	I	1×2	Single	57-64 (11.5%), <-15 dB	>17	/	0.5	no	yes
[7]	I	1×2	Single	57-64 (11.5%), <-15 dB	>18	/	0.5	no	yes
[10]	I	2×2	Dual	3.3-3.8 (14.1%), <-15 dB	>20	>25	0.53×0.71	yes	no
[12]	I	1×2	Single	3.5-3.53 (0.85%), <-10 dB	>20	/	0.4	yes	no
[16]	II	2×2	Single	2.58-2.62 (1.5%), <-10 dB	>25	/	0.21×0.21	/	yes
[18]	II	2×2	Dual	2.4-2.5 (4%), <-10 dB	>20	>30	0.5×0.5	no	/
[21]	III	1×2	Single	5.75-5.85 (1.7%), <-10 dB	>35		0.28	yes	no
[22]	III	1×2	Single	5.1-5.3 (3.8%), <-10 dB	>35		0.34	/	yes
[25]	IV	2×2	Dual	4.8-5.2 (8%), <-10 dB	>25	>28	0.62×0.62	no	/
This work	III	>3×3	Dual	3.3-4.5 (30.8%), <-15 dB	>20	>22	0.56×0.56	yes	yes

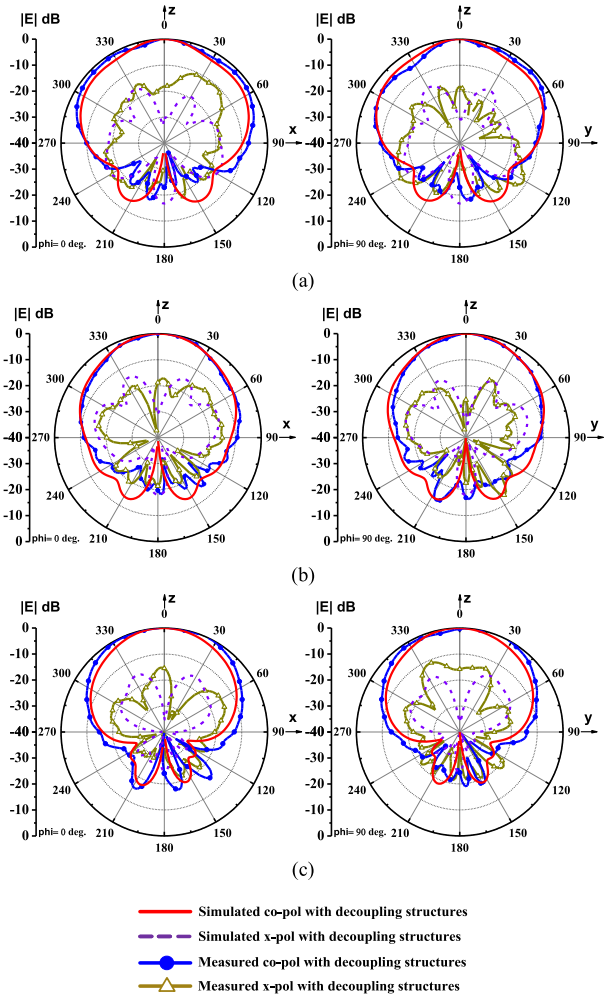

FIGURE 22. Measured radiation patterns of the center antenna element of the MIMO antenna at: (a) 3.3 GHz, (b) 3.9 GHz, and (c) 4.5 GHz.

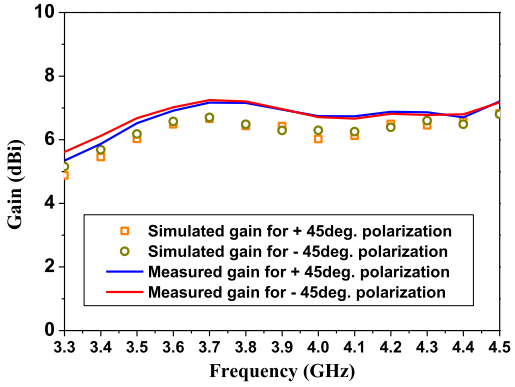

FIGURE 23. Gain of the center antenna element of the MIMO antenna.

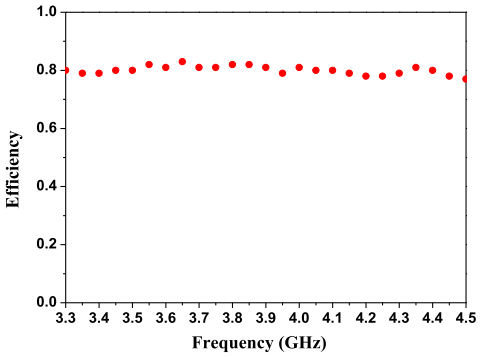

FIGURE 24. Efficiency of the center antenna element of the MIMO antenna.

can be well embedded in the MIMO antenna, which causes no extra increase in the antenna volume.

Investigations on the decoupling structures presented in recent publications have been carried out. There are roughly four kinds of decoupling methods that can be applied in M-MIMO antennas, which are metamaterial structures (Type I), decoupling networks (Type II), resonating metal decoupling structures (Type III) and decoupling ground (Type IV). Those decoupling structures have been compared in terms of array configuration (Array Config.), bandwidth for $|S11| < -10$ dB or <-15 dB (BW), dual-polarization

or not (Pol.), co-pol. mutual coupling (Co-pol.), cross-pol. mutual coupling (X-pol.), the element spacing, whether radiation pattern distortion alleviated (RPDA) or not, and whether embeddable or not (Embeddable). The comparison is listed in Table 1. Because a metasurface is usually made up of numbers of metallic cells, occupying a large space, the employment of metasurfaces may cause size increase in M-MIMO antennas. For decoupling networks, it is not easy to achieve good decoupling performance over a wide band [16], [18]. Besides, the implementation of the decoupling networks could be complicated and may not be adequate to be installed on a large scale in a M-MIMO antenna. The resonating metal decoupling structures may have large size and thus cannot be directly used for dual-polarized MIMO antenna. To the best of the authors' knowledge, only the decoupling structures presented in [10], [18] and [25] claim M-MIMO antenna applications. However, they can only afford a bandwidth less than 16%, which is not wide enough for 5G applications. It is found that the proposed decoupling structure can operate over a bandwidth of 30.8%. For the perspective view of practical applications, in addition to wide bandwidth, the compact configuration is essentially important. Our decoupling structure can be totally embedded in the M-MIMO antenna within a compact element spacing of $0.56\lambda_c$, causing no increase in the antenna volume. The proposed decoupling structure exhibits advantages of wide bandwidth, radiation pattern distortion alleviation, embeddable capability, and dual-polarization for M-MIMO applications.

VI. CONCLUSION

This paper proposes an embeddable decoupling structure for reducing the mutual couplings for M-MIMO antennas. By introducing parasitic metal strips around the antenna elements, additional couplings are provided to counterbalance the original mutual coupling between antenna elements in a M-MIMO antenna. The proposed decoupling structure features a simple configuration that can be easily embedded in a compact M-MIMO antenna, avoiding any volume increase. A 3×3 MIMO antenna for the 5G bands from 3.3-4.5 GHz is developed using the proposed decoupling structure. It is shown that the decoupling structure can effectively reduce the mutual coupling and alleviate the deterioration on radiation patterns, which is suitable for sub-6 GHz massive MIMO antenna applications.

APPENDIX

The mutual impedance of Dip 1 and Dip 2 is given in [12] as following:

$$Z_{12} = Z_{21} = R_{21} + X_{21}i \tag{A1}$$

where

$$R_{21} = -15\cos\beta d \begin{bmatrix} -2Ci2\beta d + Ci2\beta(d-L) \\ +Ci2\beta(d+L) - \ln\left(\dfrac{d^2-L^2}{d^2}\right) \end{bmatrix} + 15\sin\beta d[2Si2\beta d - Si2(d-L) - Si2\beta(d+L)](\Omega) \tag{A2}$$

$$X_{21} = -15\cos\beta d \begin{bmatrix} 2Si\beta d - Si2\beta(d-L) \\ -Si2\beta(d+L) \end{bmatrix} + (15\sin\beta d) \begin{bmatrix} 2Ci2\beta d - Ci2\beta\,(d-L) \\ -Ci2\beta(d+L) - \ln\left(\dfrac{d^2-L^2}{d^2}\right) \end{bmatrix} (\Omega) \tag{A3}$$

with

$$CiA = \int_0^A \frac{\cos t}{t} dt$$
$$SiA = \int_0^A \frac{\sin t}{t} dt \tag{A4}$$

The mutual impedance of Dip 1 (or Dip 2) and Dip 3 is given in [12] as following:

$$Z_{13} = Z_{31} = Z_{32} = Z_{23} = R_{31} + X_{31}i \tag{A5}$$

where

$$R_{31} = -15\cos\beta d \begin{pmatrix} -2CiA - 2CiA' + CiB \\ +CiB' + CiC + CiC' \end{pmatrix} + 15\sin\beta d \begin{pmatrix} 2SiA - 2SiA' - SiB \\ +SiB' - SiC + SiC' \end{pmatrix} (\Omega) \tag{A6}$$

$$X_{31} = -15\cos\beta d \begin{pmatrix} 2SiA + SiA' - SiB \\ -SiB' - SiC - SiC' \end{pmatrix} + 15\sin\beta d \times \begin{pmatrix} 2CiA - 2CiA' - CiB \\ +CiB' - CiC + CiC' \end{pmatrix} (\Omega) \tag{A7}$$

with

$$A = \beta\left(\sqrt{d_2^2 + h^2} + h\right)$$
$$A' = \beta\left(\sqrt{d_2^2 + h^2} - h\right)$$
$$B = \beta\left[\sqrt{d_2^2 + (h-L)^2} + (h-L)\right]$$
$$B' = \beta\left[\sqrt{d_2^2 + (h-L)^2} - (h-L)\right]$$
$$C = \beta\left[\sqrt{d_2^2 + (h+L)^2} + (h+L)\right]$$
$$C' = \beta\left[\sqrt{d_2^2 + (h+L)^2} - (h+L)\right] \tag{A8}$$

REFERENCES

[1] R. Janaswamy, "Effect of element mutual coupling on the capacity of fixed length linear arrays," *IEEE Antennas Wireless Propag. Lett.*, vol. 1, pp. 157–160, 2002.

[2] H. Quoc Ngo, E. G. Larsson, and T. L. Marzetta, "Energy and spectral efficiency of very large multiuser MIMO systems," *IEEE Trans. Commun.*, vol. 61, no. 4, pp. 1436–1449, Apr. 2013.

[3] X. Chen, S. Zhang, and Q. Li, "A review of mutual coupling in MIMO systems," *IEEE Access*, vol. 6, pp. 24706–24719, 2018.

[4] X. Mei and K.-L. Wu, "How low does mutual coupling need to be for MIMO antennas," in *Proc. IEEE Int. Symp. Antennas Propag. USNC/URSI Nat. Radio Sci. Meeting*, Boston, MA, USA, Jul. 2018, pp. 1579–1580.

[5] A. Dadgarpour, B. Zarghooni, B. S. Virdee, T. A. Denidni, and A. A. Kishk, "Mutual coupling reduction in dielectric resonator antennas using metasurface shield for 60-GHz MIMO systems," *IEEE Antennas Wireless Propag. Lett.*, vol. 16, pp. 477–480, 2017.

[6] R. Hafezifard, M. Naser-Moghadasi, J. Rashed Mohassel, and R. A. Sadeghzadeh, "Mutual coupling reduction for two closely spaced meander line antennas using metamaterial substrate," *IEEE Antennas Wireless Propag. Lett.*, vol. 15, pp. 40–43, 2016.
[7] M. Farahani, J. Pourahmadazar, M. Akbari, M. Nedil, A. R. Sebak, and T. A. Denidni, "Mutual coupling reduction in millimeter-wave MIMO antenna array using a metamaterial polarization-rotator wall," *IEEE Antennas Wireless Propag. Lett.*, vol. 16, pp. 2324–2327, 2017.
[8] M.-C. Tang, Z. Chen, H. Wang, M. Li, B. Luo, J. Wang, Z. Shi, and R. W. Ziolkowski, "Mutual coupling reduction using meta-structures for wideband, dual-polarized, and high-density patch arrays," *IEEE Trans. Antennas Propag.*, vol. 65, no. 8, pp. 3986–3998, Aug. 2017.
[9] B. Yin, X. Feng, and J. Gu, "A metasurface wall for isolation enhancement: Minimizing mutual coupling between MIMO antenna elements," *IEEE Antennas Propag. Mag.*, vol. 62, no. 1, pp. 14–22, Feb. 2020.
[10] K.-L. Wu, C. Wei, X. Mei, and Z.-Y. Zhang, "Array-antenna decoupling surface," *IEEE Trans. Antennas Propag.*, vol. 65, no. 12, pp. 6728–6738, Dec. 2017.
[11] F. Liu, J. Guo, L. Zhao, X. Shen, and Y. Yin, "A meta-surface decoupling method for two linear polarized antenna array in Sub-6 GHz base station applications," *IEEE Access*, vol. 7, pp. 2759–2768, 2019.
[12] H. Luan, C. Chen, W. Chen, L. Zhou, H. Zhang, and Z. Zhang, "Mutual coupling reduction of closely E/H-plane coupled antennas through meta-surfaces," *IEEE Antennas Wireless Propag. Lett.*, vol. 18, no. 10, pp. 1996–2000, Oct. 2019.
[13] J. Sui and K.-L. Wu, "A general T-Stub circuit for decoupling of two dual-band antennas," *IEEE Trans. Microw. Theory Techn.*, vol. 65, no. 6, pp. 2111–2121, Jun. 2017.
[14] J. W. Sui and K. L. Wu, "Self-curing decoupling technique for two inverted-F antennas with capacitive loads," *IEEE Trans. Antennas Propag.*, vol. 66, no. 3, pp. 1093–1100, Mar. 2018.
[15] M. Li, L. Jiang, and K. L. Yeung, "Novel and efficient parasitic decoupling network for closely coupled antennas," *IEEE Trans. Antennas Propag.*, vol. 67, no. 6, pp. 3574–3585, Jun. 2019.
[16] L. Zhao and K.-L. Wu, "A decoupling technique for four-element symmetric arrays with reactively loaded dummy elements," *IEEE Trans. Antennas Propag.*, vol. 62, no. 8, pp. 4416–4421, Aug. 2014.
[17] H. Meng and K.-L. Wu, "An LC decoupling network for two antennas working at low frequencies," *IEEE Trans. Microw. Theory Techn.*, vol. 65, no. 7, pp. 2321–2329, Jul. 2017.
[18] Y.-M. Zhang, S. Zhang, J.-L. Li, and G. F. Pedersen, "A Transmission-Line-Based decoupling method for MIMO antenna arrays," *IEEE Trans. Antennas Propag.*, vol. 67, no. 5, pp. 3117–3131, May 2019.
[19] M. Li, L. Jiang, and K. L. Yeung, "A novel wideband decoupling network for two antennas based on the wilkinson power divider," *IEEE Trans. Antennas Propag.*, vol. 68, no. 7, pp. 5082–5094, Jul. 2020, doi: 10.1109/TAP.2020.2981679.
[20] M. Li, J. M. Yasir, K. L. Yeung, and L. Jiang, "A novel dual-band decoupling technique," *IEEE Trans. Antennas Propag.*, vol. 68, no. 10, pp. 6923–6934, Oct. 2020, doi: 10.1109/TAP.2020.2995314.
[21] H. Qi, L. Liu, X. Yin, H. Zhao, and W. J. Kulesza, "Mutual coupling suppression between two closely spaced microstrip antennas with an asymmetrical coplanar strip wall," *IEEE Antennas Wireless Propag. Lett.*, vol. 15, pp. 191–194, 2016.
[22] C.-H. Park and H.-W. Son, "Mutual coupling reduction between closely spaced microstrip antennas by means of H-shaped conducting wall," *Electron. Lett.*, vol. 52, no. 13, pp. 1093–1094, Jun. 2016.
[23] M. Li, B. G. Zhong, and S. W. Cheung, "Isolation enhancement for MIMO patch antennas using near-field resonators as coupling-mode transducers," *IEEE Trans. Antennas Propag.*, vol. 67, no. 2, pp. 755–764, Feb. 2019.
[24] S. Zhang, X. M. Chen, and G. F. Pedersen, "Mutual coupling suppression with decoupling ground for massive MIMO antenna arrays," *IEEE Trans. Antennas Propag.*, vol. 68, no. 8, pp. 7273–7274, Aug. 2019.
[25] J. D. Kraus and R. J. Marhefkas, "Self and mutual impedances," in *Antennas: For All Applications*, 3rd ed. New York, NY, USA: McGraw-Hill, 2002, ch. 13, sec. 6, vol. 11, pp. 448–459.
[26] Y. Cui, R. Li, and P. Wang, "A novel broadband planar antenna for 2G/3G/LTE base stations," *IEEE Trans. Antennas Propag.*, vol. 61, no. 5, pp. 2767–2774, May 2013.

YUE QIN received the B.S. degree in electronic information engineering and the M.S. degree in electromagnetic field and microwave technology from the Communication University of China, Beijing, China, in 2013 and 2016, respectively. He is currently pursuing the Ph.D. degree in communication and information system with the South China University of Technology, Guangzhou, China. His research interests include antenna decoupling techniques, wideband base station antenna design, and large-scale massive multiple-input multiple-output antenna array for advanced wireless communications.

RONGLIN LI (Senior Member, IEEE) received the B.S. degree in electrical engineering from Xi'an Jiaotong University, China, in 1983, and the M.S. and Ph.D. degrees in electrical engineering from Chongqing University, in 1990 and 1994, respectively. From 1983 to 1987, he worked as an Assistant Electrical Engineer with Yunnan Electric Power Research Institute. From 1994 to 1996, he was a Postdoctoral Research Fellow with Zhejiang University, China, where he became a Professor, in 1998. In 1997, he visited Hosei University, Japan, as an HIF (Hosei International Fund) Research Fellow. In 1999, he visited the University of Utah, USA, as a Research Associate. In 2000, he worked as a Research Fellow with the Queen's University of Belfast, U.K. Since 2001, he has been a Research Scientist with the Georgia Institute of Technology, USA. He is currently an Endowed Professor with the South China University of Technology. He has published more than 100 articles in refereed journals and conference proceedings, and three book chapters. His current research interests include new design techniques for antennas in mobile and satellite communication systems, phased arrays and smart antennas for radar applications, wireless sensors and RFID technology, electromagnetics, and information theory. He is a member of the IEEE International Compumag Society. He was a member of the technical program committee of the IEEE-IMS 2008–2012 Symposia and the session chair of several IEEE-APS Symposia. He was a recipient of the 2009 Georgia Tech-ECE Research Spotlight Award. He currently serves as an Editor of *ETRI Journal* and a reviewer for a number of international journals, including the IEEE Transactions on Antennas and Propagation, IEEE Antennas and Wireless Propagation Letters, IEEE Microwave and Wireless Components Letters, *IET Microwaves, Antennas & Propagation*, *Progress in Electromagnetics Research*, *Journal of Electromagnetic Waves and Applications*, and international journal of *Wireless Personal Communications*.

YUEHUI CUI (Member, IEEE) received the B.S. degree in information science and technology from Sun Yat-sen University, Guangzhou, China, in 2009, and the Ph.D. degree in electronic and information engineering from the South China University of Technology, Guangzhou, in 2014. She is currently working as an Associate Professor with the South China University of Technology. Her research interests include base station antennas, massive MIMO antennas, and active antennas.